Journal of Power Sources 196 (2011) 6884–6888

Contents lists available at ScienceDirect

Journal of Power Sources

journal homepage: www.elsevier.com/locate/jpowsour

Short communication

Thermal stability of $Li_{1-y}Ni_xMn_{(1-x)/2}Co_{(1-x)/2}O_2$ layer-structured cathode materials used in Li-Ion batteries

Hiroaki Konishi*, Toyotaka Yuasa, Masanori Yoshikawa

Hitachi Research Laboratory, Hitachi Ltd., 7-1-1 Ohmika-cho, Hitachi, Ibaraki 319-1292, Japan

ARTICLE INFO

Article history:
Received 11 August 2010
Received in revised form
28 December 2010
Accepted 7 January 2011
Available online 19 January 2011

Keywords:
Lithium batteries
Positive electrode
Thermal stability
Oxygen release
Structure change

ABSTRACT

In order to develop safe lithium-ion batteries using Ni-based cathode active materials, such as $LiNi_xMn_{(1-x)/2}Co_{(1-x)/2}O_2$, thermal stability is one of the most important requirements. We used XRD and TDS-MS in the first step of our study to elucidate the thermal stability and to improve it under anomalous high temperature conditions. We investigated the relationship between the thermal stability and cathode composition, especially for that of the nickel and lithium content. The XRD indicated that the crystal structure of electrochemically delithiated materials changed from a layered into a spinel structure followed by a rock-salt structure as the temperature rose. The TDS-MS indicated that these changes coincided with the release of oxygen from the cathode materials. We found that decreasing the lithium content and increasing the nickel content made the temperature of the crystal structure change and oxygen release lower, and thus, influenced the cathode composition.

1. Introduction

A lot more attention than ever before is being paid to the Ni-based cathode active materials used in lithium-ion batteries. There are two reasons for this. One is the concern about the expensive and changeable cost of Co-based materials, and the other is the expectation of new applications, such as plug-in hybrid electric vehicles (PHEV) and electric vehicles (EV), which require a higher performance than conventional applications.

Increasing the nickel content in Ni-based materials is an effective way to increase their charge-discharge capacity density [1–4]. However, increasing the nickel content causes poor thermal stability [5–8], which means there is an enhanced possibility of thermal runaway under anomalous high temperature conditions. It was reported that the crystal structure of $Li_{1-a}NiO_2$ changed from a layered into a spinel structure followed by a rock-salt structure and released oxygen as the temperature rose in $Li_{1-a}NiO_2$ [9–13], and in $Li_{1-b}NiMO_2$ (M: transition metal) [14–25]. Even if the composition of the cathode active material is precisely adjusted before the cell construction, it will certainly change during the charge-discharge process and its iteration, which means, the lithium content changes in proportion to the degree of charging or discharging. However, there is no report to clearly elucidate the thermal stability of these materials as a function of the temperatures and the composition of Ni-rich $Li_{1-a}Ni_xMn_yCo_zO_2$ cathode active materials, especially that of nickel and lithium, systematically.

Therefore, we focused on the fact that the structure change of the cathode active material is affected by not only by the nickel but also by the lithium content in this paper. So, we systematically studied the relationship between them. We report on the influence of the nickel and lithium contents of $Li_{1-y}Ni_xMn_{(1-x)/2}Co_{(1-x)/2}O_2$ on the thermal stability using X-ray diffraction (XRD) and thermal desorption spectrometry-mass spectrometry (TDS-MS) as the first step toward better understanding the reaction mechanism for the materials and to improve their thermal stability, intending to use them as the cathode active material in lithium-ion batteries with improved safety.

2. Experimental

Three $LiNi_xMn_{(1-x)/2}Co_{(1-x)/2}O_2$ ($x = 1/3$, 0.6, 0.8) samples were prepared by firing a mixture of lithium hydroxide, nickel oxide, cobalt oxide, and manganese oxide in air or oxygen atmosphere at high temperatures for 10 h followed by annealing at 600 °C for 10 h. The exact temperatures used and the atmosphere were 1000 °C in air for $x = 1/3$, 900 °C in oxygen for $x = 0.6$, and 850 °C in oxygen for $x = 0.8$, which had been optimized through some preliminary experimentation.

Using the samples mentioned above, we also prepared a cathode containing active materials denoted as $Li_{1-y}Ni_xMn_{(1-x)/2}Co_{(1-x)/2}O_2$ by using the electrochemical delithiation process. First, the cathode was formed on aluminum foil by

* Corresponding author. Tel.: +81 294 52 5111x6089; fax: +81 294 52 7636.
E-mail address: hiroaki.konishi.yj@hitachi.com (H. Konishi).

0378-7753/$ – see front matter © 2011 Elsevier B.V. All rights reserved.
doi:10.1016/j.jpowsour.2011.01.016

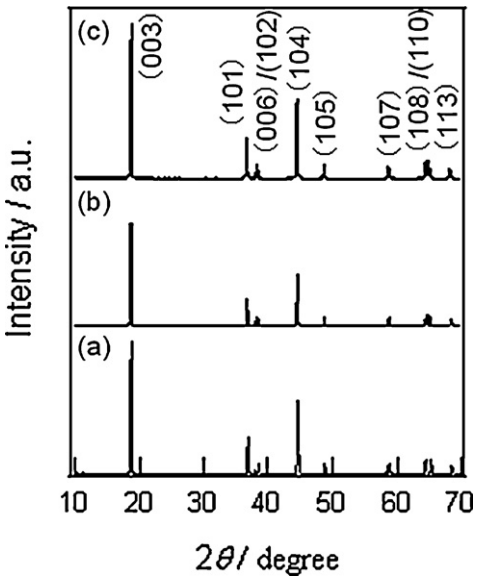

Fig. 1. XRD patterns of $LiNi_xMn_{(1-x)/2}Co_{(1-x)/2}O_2$ (a) $x = 1/3$, (b) $x = 0.6$, and (c) $x = 0.8$.

blade coating a slurry consisting of the active material, carbon, polyvinylidene difluoride (PVDF) (85:10:5 wt.%), and N-methyl pyrrolidone (NMP) solvent. Then, they were dried, pressed, and cut. The delithiated electrodes were prepared according to the following process. The test cells were assembled with the cathode, a lithium metal used as the anode, a microporous polypropylene separator, and 1 M $LiPF_6$ in a mixed solvent of ethylene carbonate (EC), ethyl methyl carbonate (EMC), and dimethyl carbonate (DMC) in an argon glove box. The cells were charged and discharged at a C/20 rate between 3.0 and 4.3 V. A cathode containing $LiNi_xMn_{(1-x)/2}Co_{(1-x)/2}O_2$ ($x = 1/3$, 0.6, 0.8) was charged to a prescribed composition ($y = 0.4$, 0.6, 0.8) at a C/20 rate of constant current. The electrodes were removed from the cells after charging, washed with DMC, and then dried. They were heated in an argon atmosphere for 1 h at 150–400 °C to expose them to anomalous high temperatures that might be caused under different kinds of unsafe conditions, and cooled to room temperature.

XRD was used to identify the crystal structures of the prepared samples before and after being heated at high temperatures, using a Rigaku diffractometer (Rint-2200 Ultima III) with a graphite monochromator and Cu Kα radiation operated at 40 kV and 40 mA. The diffraction angles were scanned from 10 to 70° using a step scan method with a 0.02° step and a counting time of 1.5 s per step. The same method as that for the XRD samples was used to prepared the ones for the TDS-MS (ESCO, Ltd., EMD-WA-1000); the charged $Li_{1-y}Ni_xMn_{(1-x)/2}Co_{(1-x)/2}O_2$ ($x = 1/3$, 0.6, 0.8; $y = 0.4$, 0.6, 0.8) electrodes were set in the TDS-MS sample chamber and heated to 400 °C in a vacuum at a rate of 5 °C/min. The released oxygen was detected using a quadrupole mass spectrometer with a 0.02 s step.

3. Results and discussion

3.1. Crystal structure of $LiNi_xMn_{(1-x)/2}Co_{(1-x)/2}O_2$ ($x = 1/3$, 0.6, 0.8)

Fig. 1 shows the XRD patterns of $LiNi_xMn_{(1-x)/2}Co_{(1-x)/2}O_2$ ($x = 1/3$, 0.6, 0.8). All the peaks were assigned to the hexagonal α-$NaFeO_2$ structure of a $R3m$ space group. The clear peak split of (1 0 8) and (1 1 0) was observed for all the samples, implying the formation of a well-ordered crystalline layered structure.

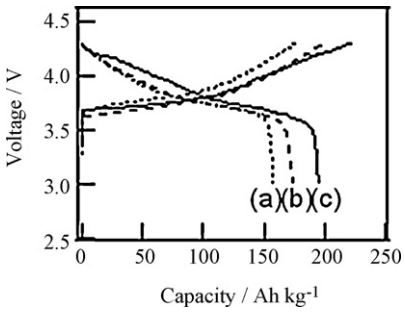

Fig. 2. Initial charge and discharge capacity densities of LiNixMn(1-x)/2Co(1-x)/2O2 ($x = 1/3$, 0.6, 0.8) within voltage range of 3.0–4.3 V at rate of C/20 (a) $x = 1/3$, (b) $x = 0.6$, and (c) $x = 0.8$.

3.2. Charge-discharge capacities of $LiNi_xMn_{(1-x)/2}Co_{(1-x)/2}O_2$ ($x = 1/3$, 0.6, 0.8)

Fig. 2 shows the charge-discharge curves for the first cycle of the cathode with $LiNi_xMn_{(1-x)/2}Co_{(1-x)/2}O_2$ ($x = 1/3$, 0.6, 0.8). They had good reversibility: the Coulombic efficiencies of the electrodes for the first cycle were 87–90%, and those for the second cycle were 99%. In addition, the voltage difference between the first and second charging curves was less than 0.2 V for all three electrodes. Table 1 lists the initial charge-discharge capacity densities of the $LiNi_xMn_{(1-x)/2}Co_{(1-x)/2}O_2$ ($x = 1/3$, 0.6, 0.8) electrodes when applying a constant current of C/20 within the voltage range of 3.0–4.3 V along with the Coulombic efficiencies for the first cycle discussed above. The discharge capacity density increased as the nickel content increased. These results indicate that nickel is the main redox species of the transition metals in the tested voltage range.

3.3. Crystal structure of $Li_{1-y}Ni_xMn_{(1-x)/2}Co_{(1-x)/2}O_2$ ($x = 1/3$, 0.6, 0.8; $y = 0.4$, 0.6, 0.8) at high temperatures

XRD was used to elucidate the crystal structure change of electrochemically delithiated $Li_{1-y}Ni_xMn_{(1-x)/2}Co_{(1-x)/2}O_2$ ($x = 1/3$, 0.6, 0.8; $y = 0.4$, 0.6, 0.8) electrodes. Figs. 3–5 show the XRD patterns for those heated at 150–400 °C. These results are also summarized in Table 2.

3.3.1. $x = 1/3$

Fig. 3 shows the XRD patterns of the $Li_{1-y}Ni_{1/3}Mn_{1/3}Co_{1/3}O_2$ ($y = 0.4$, 0.6, 0.8) electrodes heated at 150–400 °C. For $y = 0.4$ and at 150 °C, all the peaks were assigned to the layered structure of the $R3m$ space group. From 150 to 400 °C, the (1 0 8) and (1 1 0) peaks, which appeared at around 65°, merged. At 350 °C, a new peak at $2\theta = 31°$ emerged. This peak is characteristic of the spinel structure of the $Fd3m$ space group. This result indicates that the layered structure is stable below 300 °C and begins to change into a spinel structure at 350 °C. The same change arose for $y = 0.6$. However, that for $y = 0.8$ began at as low as 300 °C.

Table 1
Initial charge and discharge capacities and Coulombic efficiencies of $LiNi_xMn_{(1-x)}/_2Co_{(1-x)}/_2O_2$ ($x = 1/3$, 0.6, 0.8) within voltage range of 3.0–4.3 V at rate of C/20.

x	Charge capacity (Ah kg^{-1})	Discharge capacity (Ah kg^{-1})	Coulombic efficiency (%)
1/3	176	158	89.8
0.6	199	175	87.9
0.8	223	195	87.4

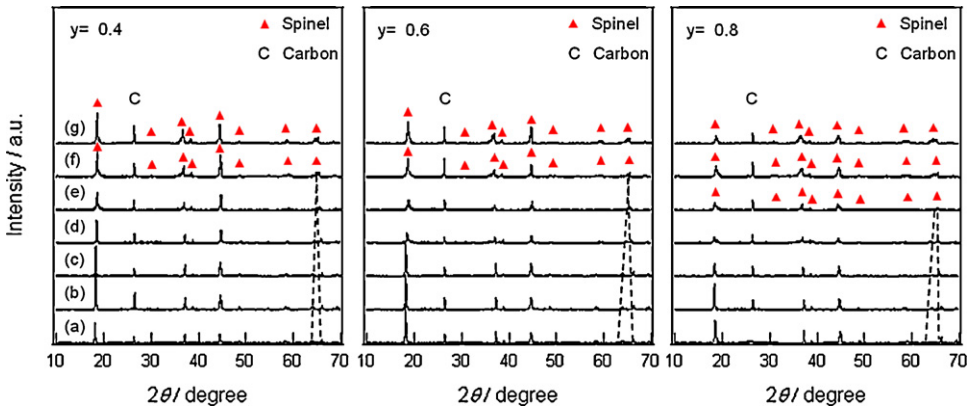

Fig. 3. XRD patterns of $Li_{1-y}Ni_{1/3}Mn_{1/3}Co_{1/3}O_2$ (y = 0.4, 0.6, 0.8) electrodes (a) as prepared, and heated at (b) 150 °C, (c) 200 °C, (d) 250 °C, (e) 300 °C, (f) 350 °C, and (g) 400 °C.

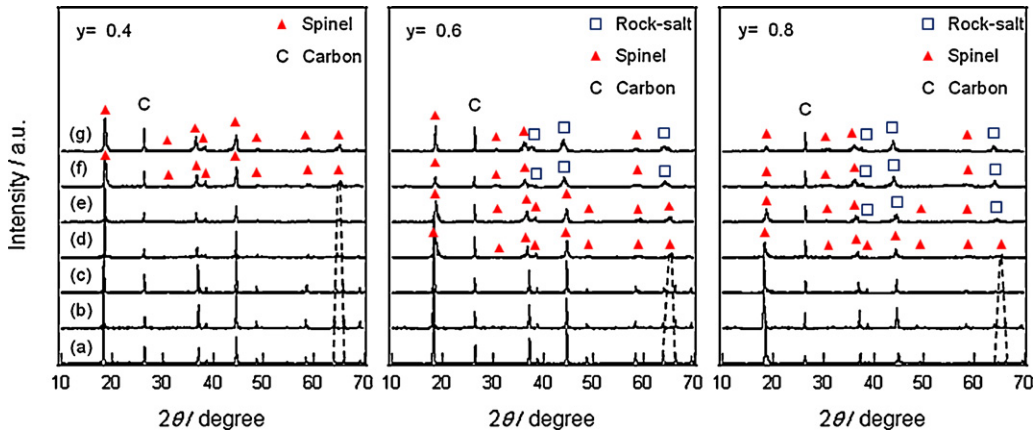

Fig. 4. XRD patterns of $Li_{1-y}Ni_{0.6}Mn_{0.2}Co_{0.2}O_2$ (y = 0.4, 0.6, 0.8) electrodes (a) as prepared, and heated at (b) 150 °C, (c) 200 °C, (d) 250 °C, (e) 300 °C, (f) 350 °C, and (g) 400 °C.

3.3.2. $x = 0.6$

Fig. 4 shows the XRD patterns of the $Li_{1-y}Ni_{0.6}Mn_{0.2}Co_{0.2}O_2$ (y = 0.4, 0.6, 0.8) electrodes heated at 150–400 °C. For y = 0.4, all the changes were almost identical to those for x = 1/3 and y = 0.4, 0.6 mentioned above.

The results for y = 0.6 were similar to those for y = 0.4 except at two points: one was that the structural change from a layered into a spinel structure occurred at as low as 250 °C, and the other is that the rock-salt structure of the Fm3m space group emerged at 350 °C. All the results for y = 0.8 were similar to those for y = 0.6 with a low temperature shift of 50 °C for the emergence of the rock-salt structure, as listed in Table 2.

3.3.3. $x = 0.8$

Fig. 5 shows the XRD patterns of the $Li_{1-y}Ni_{0.8}Mn_{0.1}Co_{0.1}O_2$ (y = 0.4, 0.6, 0.8) electrodes heated at 150–400 °C. The crystal structure changes occurred in the same sequence as that in the former two cases, x = 1/3 and x = 0.6: a layered into a spinel structure followed by the coexistence of a spinel and a rock-salt structure. The difference here is in the temperatures at which the changes occurred. Namely, we found that the tendency for a higher nickel and a lower lithium content to lower the structure-changing temperatures is valid even for these compositions, which is explicitly shown in Fig. 5 and Table 2.

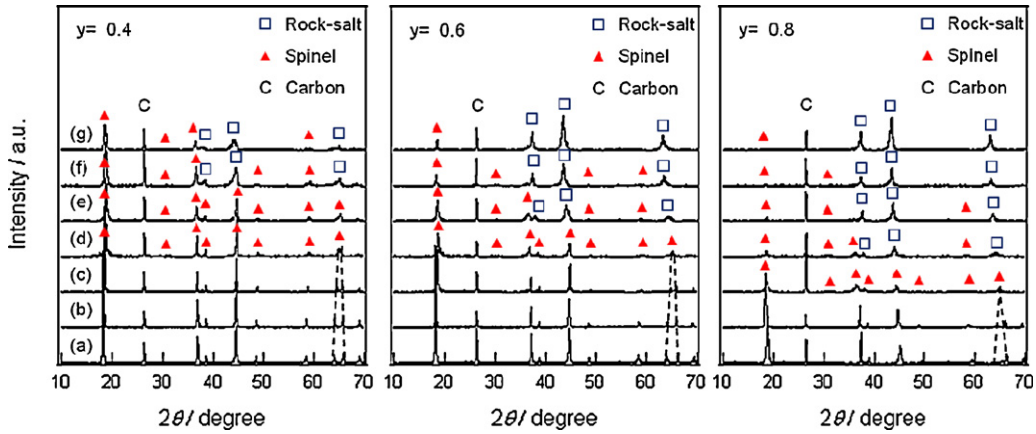

Fig. 5. XRD patterns of $Li_{1-y}Ni_{0.8}Mn_{0.1}Co_{0.1}O_2$ (y = 0.4, 0.6, 0.8) electrodes (a) as prepared, and heated at (b) 150 °C, (c) 200 °C, (d) 250 °C, (e) 300 °C, (f) 350 °C, and (g) 400 °C.

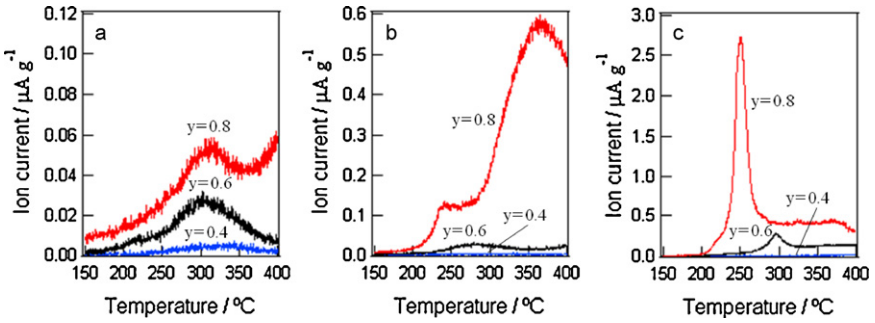

Fig. 6. Oxygen release behaviors of $Li_{1-y}Ni_xMn_{(1-x)/2}Co_{(1-x)/2}O_2$ (a) $x = 1/3$, (b) $x = 0.6$, and (c) $x = 0.8$.

Table 2
Crystal structures of $Li_{1-y}Ni_xMn_{(1-x)/2}Co_{(1-x)/2}O_2$ (x = 1/3, 0.6, 0.8; y = 0.4, 0.6, 0.8) from 25 to 400 °C.

x	y	Temperature (°C)						
		25	150	200	250	300	350	400
1/3	0.4	L	L	L	L	L	S	S
	0.6	L	L	L	L	L	S	S
	0.8	L	L	L	L	S	S	S
0.6	0.4	L	L	L	L	L	S	S
	0.6	L	L	L	S	S	S, R	S, R
	0.8	L	L	L	S	S, R	S, R	S, R
0.8	0.4	L	L	L	S	S	S, R	S, R
	0.6	L	L	L	S	S, R	S, R	S, R
	0.8	L	L	S	S, R	S, R	S, R	S, R

L: layer, S: spinel, and R: rock-salt.

3.4. Oxygen release of $Li_{1-y}Ni_xMn_{(1-x)/2}Co_{(1-x)/2}O_2$ ($x = 1/3$, 0.6, 0.8; $y = 0.4$, 0.6, 0.8)

It is well-known that the thermal decomposition of cathode active material in lithium-ion batteries, such as layer-structured $LiMO_2$ release oxygen, will cause thermal runaway. Therefore, we intended to elucidate the oxygen release reaction of the electrochemically delithiated $Li_{1-y}Ni_xMn_{(1-x)/2}Co_{(1-x)/2}O_2$ ($x = 1/3$, 0.6, 0.8; $y = 0.4$, 0.6, 0.8) in connection with the structural change of the materials, using TDS-MS.

Fig. 6 shows the TDS-MS results from the $Li_{1-y}Ni_xMn_{(1-x)/2}Co_{(1-x)/2}O_2$ ($x = 1/3$, 0.6, 0.8; $y = 0.4$, 0.6, 0.8) electrode. The amount of oxygen release for $x = 1/3$ increased as the lithium content decreased, or namely y increased. The tendency for oxygen release for $x = 0.6$ was similar to that for $x = 1/3$, but the oxygen release for $y = 0.8$ was very large. The tendency for oxygen release for $x = 0.8$ was similar to that for $x = 1/3$ and 0.6, but the amount of oxygen release for $y = 0.8$ abruptly increased at around 250 °C. It was previously reported that the oxygen release was caused by reactions (1)–(3) shown below [9,11–13].

$0 < y < 0.5$

$$Li_{1-y}MO_2 \rightarrow (1-2y)LiMO_2 + yLiM_2O_4 \quad (1)$$

$y > 0.5$

$$Li_{1-y}MO_2 \rightarrow (2-y)/3[Li_{3(1-y)/(2-y)}M_{(2y-1)/(2-y)}][M]_2O_4 + [(2y-1)/3]O_2 \quad (2)$$

$$\rightarrow [Li_{1-y}M]O_{2-y} + [(2-y)/6]O_2 \quad (3)$$

Reactions (1)–(3) and the results shown in Fig. 6 are summarized as follows:

1) For $y = 0.4$, all the cases where $x = 1/3$, 0.6, and 0.8 substantially showed no oxygen release, which was consistent with reaction (1).
2) For $y = 0.6$ and 0.8, which are more delithiated conditions, the amount of oxygen release increased according to the delithiation, which was consistent with reactions (2) and (3).
3) In addition, for $y = 0.6$ and 0.8, the amount of oxygen release abruptly increased according to the x values from 0.6 to 0.8, which was also consistent with reactions (2) and (3).

All these results are in good correlation with Figs. 3–5 along with Table 2, which summarized the three figures. This good coincidence presents a systematic description of the thermal stability of layer-structured lithium-transition metal double oxides for the cathode active material in lithium-ion batteries denoted as $Li_{1-y}Ni_xMn_{(1-x)/2}Co_{(1-x)/2}O_2$ ($x = 1/3$, 0.6, 0.8; $y = 0.4$, 0.6, 0.8).

3.5. Thermal stability

The reason why $x = 1/3$ is not likely to change from a layered into a spinel structure is speculated to be as follows. A $[Li_{3(1-y)/(2-y)}M_{(2y-1)/(2-y)}][M]_2O_4$, spinel structure, has two cation sites, tetrahedral and octahedral. When the crystal structure changes from a layered into a spinel structure, some of the cations have to move from the octahedral into the tetrahedral sites according to reaction (1). A nickel ion with a high valence is unstable, and is likely to decrease the valence accompanied by the oxygen release. So, the bond between the nickel and oxygen breaks and the nickel ion moves from the octahedral site into the tetrahedral one according to reaction (2) [11,19].

For a high nickel content and y over 0.5, the amount of nickel moving from the octahedral into the tetrahedral sites is large enough to change the structure from a layered into a spinel structure, and the oxygen is released according to reaction (2) and followed by that according to reaction (3).

In addition, the reason why high nickel content materials, $x = 0.6$ and $x = 0.8$, are likely to change from a spinel into a rock-salt structure at lower temperatures is attributed to the fact that a spinel structure is unstable for a high nickel content material. Namely, the valence of transition metals for a spinel structure, $[Li_{3(1-y)/(2-y)}M_{(2y-1)/(2-y)}][M]_2O_4$, are a mixture of 3^+ and 4^+ at which nickel is unstable. However, the valence of Ni became near 2^+ and stabilized when the structure changed into the rock-salt, thus the structure remained unchanged.

The discussion mentioned above showed a rather clear depiction on the crystal structure change of $Li_{1-y}Ni_xMn_{(1-x)/2}Co_{(1-x)/2}O_2$ ($x = 1/3$, 0.6, 0.8; $y = 0.4$, 0.6, 0.8) in connection with the composition and temperatures. However, some points have still not been explicitly proved and further complementary data such as that on the valence state of the transition metals is necessary to complete the depiction. Although it has been stated that the high nickel content in layer-structured $LiMO_2$ causes thermal instability, Fig. 6 shows that such materials are stable as long as they have a less delithiated state of less than $y = 0.4$. Therefore, the thermal stability issue does not concern that for the discharged state but that for

the charged and especially the overcharged states. From a practical point of view, knowing how to control the thermal stability even in the overcharged state is the key to taking advantage of the high capacity densities of high nickel content cathode active materials, as shown in Table 1. We expect that the partial substitution of a hetero atom for nickel will surely help to stabilize the crystal structure by analogy with the case of $LiMn_2O_4$ [26,27].

4. Conclusion

$LiNi_xMn_{(1-x)/2}Co_{(1-x)/2}O_2$ ($x = 1/3$, 0.6, 0.8) was prepared using a solid state process. The discharge capacity densities of the prepared samples increased according to the nickel content in the composition formulae. The thermal stabilities of the electrochemically delithiated materials of $Li_{1-y}Ni_xMn_{(1-x)/2}Co_{(1-x)/2}O_2$ ($x = 1/3$, 0.6, 0.8; y= 0.4, 0.6, 0.8) were elucidated by XRD and TDS-MS. Decreasing the lithium content and increasing the nickel content made the temperature of the crystal structure decrease. The change in the crystal structure accompanied the release of oxygen. We attributed the reason for the instability of the high nickel content cathode to the instability of the high valence of Ni, Ni^{3+} and Ni^{4+}. Therefore, the layered structure changes into a spinel one followed by rock-salt structure accompanying the oxygen release, and the nickel valence decreases. All these results suggest that it is essential to control the nickel valence in order to utilize the high capacity density of these materials.

Acknowledgements

This work was supported by the New Energy and Industrial Technology Development Organization (NEDO) of Japan as a part of the Li-EAD Project. The authors would like to thank those who participated in the projects.

They also would like to thank Dr. T. Horiba of Shin-Kobe Electric Machinery Co., Ltd. for his encouraging and suggestive discussions on this paper.

References

[1] J.R. Dahn, U. von Sacken, M.W. Juzkow, H. Al-Janaby, J. Electrochem. Soc. 138 (1991) 2207–2211.
[2] T. Ohzuku, A. Ueda, M. Nagayama, J. Electrochem. Soc. 148 (1993) 1862–1870.
[3] K.-S. Lee, S.-T. Myung, K. Amine, H. Yashiro, Y.-K. Sun, J. Electrochem. Soc. 154 (2007) A971–A977.
[4] A. Deb, U. Bergmann, S.P. Cramer, E.J. Cairns, J. Electrochem. Soc. 154 (2007) A534–A541.
[5] J.R. Dahn, E.W. Fuller, M. Obrovac, U. Von Sacken, Solid State Ionics 69 (1994) 265–270.
[6] D.D. MacNeil, Z. Lu, Z. Chen, J.R. Dahn, J. Power Sources 108 (2002) 8–14.
[7] H. Arai, M. Tsuda, K. Saito, M. Hayashi, Y. Sakurai, J. Electrochem. Soc. 149 (2002) A401–A406.
[8] S. Jouanneau, D.D. MacNeil, Z. Lu, S.D. Beattie, G. Murphy, J.R. Dahn, J. Electrochem. Soc. 150 (2003) A1299–A1304.
[9] H. Arai, S. Okada, Y. Sakurai, J. Yamaki, Solid State Ionics 109 (1998) 295–302.
[10] H. Arai, Y. Sakurai, J. Power Sources 81–82 (1999) 401–405.
[11] M. Guilmard, L. Croguennec, D. Denux, C. Delmas, Chem. Mater. 15 (2003) 4476–4483.
[12] K.-K. Lee, W.-S. Yoon, K.-B. Kim, K.-Y. Lee, S.-T. Hong, J. Power Sources 97–98 (2001) 321–325.
[13] K.-K. Lee, W.-S. Yoon, K.-B. Kim, K.-Y. Lee, S.-T. Hong, J. Electrochem. Soc. 148 (2001) A716–A722.
[14] K.-K. Lee, W.-S. Yoon, K.-B. Kim, J. Electrochem. Soc. 148 (2001) A1164–A1170.
[15] W.-S. Yoon, M. Balasubramanian, X.-Q. Yang, J. McBreen, J. Hanson, Electrochem. Solid State Lett. 8 (2005) A83–A86.
[16] W.-S. Yoon, K.Y. Chung, M. Balasubramanian, J. Hanson, J. McBreen, X.-Q. Yang, J. Power Sources 163 (2006) 219–222.
[17] W.-S. Yoon, J. Hanson, J. McBreen, X.-Q. Yang, Electrochem. Commun. 8 (2006) 859–862.
[18] K.-W. Nam, W.-S. Yoon, X.-Q. Yang, J. Power Sources 189 (2009) 515–518.
[19] M. Guilmard, L. Croguennec, C. Delmas, Chem. Mater. 15 (2003) 4484–4493.
[20] H. Bang, D.-H. Kim, Y.C. Bae, J. Prakash, Y.-K. Sun, J. Electrochem. Soc. 155 (2008) A952–A958.
[21] S.-T. Myung, A. Ogata, K.-S. Lee, S. Komaba, Y.-K. Sun, H. Yashiro, J. Electrochem. Soc. 155 (2008) A374–A383.
[22] I. Belharouak, D. Vissers, K. Amine, J. Electrochem. Soc. 153 (2006) A2030–A2035.
[23] I. Belharouak, W. Lu, D. Vissers, K. Amine, Electrochem. Commun. 8 (2006) 329–335.
[24] I. Belharouak, W. Lu, J. Liu, D. Vissers, K. Amine, J. Power Sources 174 (2007) 905–909.
[25] N. Yabuuchi, Y.-T. Kim, H.H. Li, Y. Shao-Horn, Chem. Mater. 20 (2008) 4936–4951.
[26] W. Baochen, X. Yongyao, F. Li, Z. Dongjiang, J. Power Sources 44 (1993) 539–546.
[27] Li. Guohua, H. IKuta, T. Uchida, M. Wakihara, J. Electrochem. Soc. 143 (1996) 178–182.